

4 *Spatial Array Processing*

The neglected borderland between two branches of knowledge is often that which best repays cultivation, or, to use a metaphor of Maxwell's, the greatest benefits may be derived from a cross fertilisation of the sciences.

Lord Rayleigh, John William Strutt, *Presidential Address to the British Association's Montreal Meeting of 1884*

4.1 Introduction

The primary goal of spatial array processing is signal enhancement and detection. In traditional SASW tests, the two-sensor data is not efficiently combined to yield maximum engineering information, as discussed in Chapter 6. The multidimensional signal processing and spectrum estimation problems generalize the one-dimensional procedures in many ways, but several important extensions and limitations must be addressed. This chapter will introduce the general multidimensional problem, and follow a path parallel to the one-dimensional problem. Since the data collection and analysis will now be dealing with three dimensions, i.e. time and two-dimensional space, most of the formulas and analysis will be framed in vector notation. The compact vector notation offers a great deal of flexibility and insight into the relationship between different multidimensional power spectrum estimators.

The chapter begins with an introduction of the primary spatial parameters through an ideal wavefield model. Spectral operators and power spectrum estimators will then be introduced and analyzed to discover how spatial array geometry, sensor characteristics, and sensor weighting functions combine to determine the final spectral output. Comparisons of a few possible array geometries are presented in Chapter 5.

4.2 Ideal Wavefield Model and Parameters

An additional parameter must be introduced to describe the spatial variation of a wavefield. The new parameter is a vector spatial frequency called wavenumber, \mathbf{k} . Temporal frequency, wave propagation phase velocity, and wavenumber completely

describe the dispersion relation and the physics of seismic surface wave propagation. Just as the natural frequency of single degree-of-freedom systems describes the natural temporal tendency of a system, wavenumber yields insight into the natural spatial tendency of the system.

Wavenumber components enter into the wave equation as complex exponential arguments and affect wave propagation in ways similar to temporal frequency. The fundamental similarity between the temporal and spatial frequency is orthogonality of monochromatic components. In fact, the orthogonality of different frequencies and wavenumbers allows the division of a temporally and spatially wideband wavefield into spectral components, including extraction and disentanglement of different seismic wave modes. The ability to determine the natural frequencies and wavenumbers yields the desired engineering parameters. The goal of all seismic surface wave experimental measurements is the determination of the natural wavenumbers of a layered system as a function of frequency. The dominant wavenumbers directly yield phase velocity estimates and are necessary to obtain attenuation coefficient estimates.

4.2.1 Ideal Wavefield

If an ideal monochromatic, unit amplitude plane wave, characterized by a single frequency ω_0 (rad/sec), single wavenumber \mathbf{k}_0 (rad/m), and, therefore, constant phase velocity, propagates past an array of sensors from a given direction θ , as shown in Figure 4.1, the wave field is given by

$$z(\mathbf{x}, t) = \exp[j(\omega_0 t - \mathbf{k}_0 \cdot \mathbf{x})] \quad (4.1)$$

where $z(\mathbf{x}, t)$ = the wave field measured at time t and vector position \mathbf{x} , and $j = \sqrt{-1}$. Planes of constant phase propagate past different positions with a time delay due to the change in spatial location. Time delays between sensors in the temporal domain give linear phase shifts in the frequency domain, yielding information about the wavenumber \mathbf{k}

$$\mathbf{k} = \frac{2\pi}{\lambda} \hat{\zeta} = \frac{\Delta\phi}{\Delta d} \hat{\zeta} \quad (4.2)$$

where λ = wavelength, $\Delta\phi$ = change in phase over the distance Δd , and $\hat{\zeta}$ is a unit vector in the direction of propagation.

Loosely, wavenumber is a spatial frequency, indicating the number of cycles per unit length that a monochromatic wave exhibits in the direction of propagation. Since the seismic surface wavefields considered in this dissertation have two spatial dimensions, the spatial frequency content of waves must be represented as a two-dimensional vector (Johnson and Dudgeon, 1993). The wavenumber easily extends to three dimensions for non-planar wavefields.

If unlimited temporal and spatial data could be collected, the wavefield in the f - \mathbf{k} domain would be given by

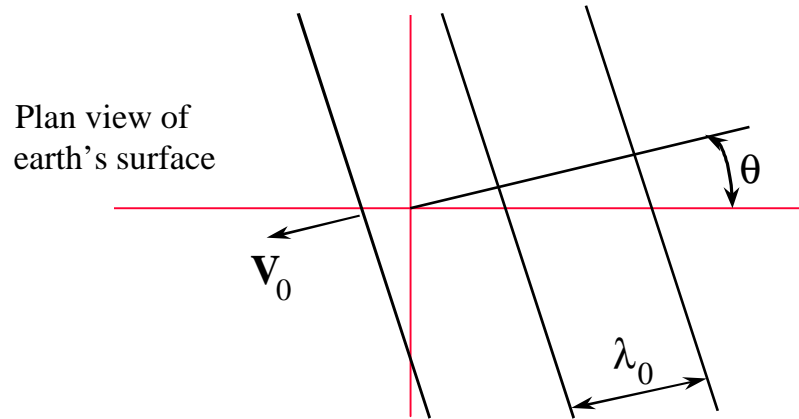


Figure 4.1 Ideal, Single Signal Wavefield. The wavenumber \mathbf{k}_0 describes the wavelength λ_0 , velocity of propagation v_0 , and direction of propagation θ .

$$Z(\mathbf{k}, \omega) = \int_{-\infty}^{+\infty} \int_{-\infty}^{+\infty} \int_{-\infty}^{+\infty} \delta(\omega - \omega_0) \delta(\mathbf{k}_x - \mathbf{k}_{0,x}) \delta(\mathbf{k}_y - \mathbf{k}_{0,y}) d\omega d\mathbf{k}_x d\mathbf{k}_y \quad (4.3)$$

i.e. a three dimensional impulse function in frequency-wavenumber space, where $\mathbf{k}_0 = k_{0,x} \cdot \hat{\mathbf{i}} + k_{0,y} \cdot \hat{\mathbf{j}}$, and $\hat{\mathbf{i}}$ and $\hat{\mathbf{j}}$ are unit vectors. Figure 4.2 shows an example line spectrum in wavenumber space.

Wavenumber is a vector quantity, exhibiting both a magnitude and a direction, and the magnitude of \mathbf{k} at a given frequency directly yields the phase velocity. Different directions and phase velocities must be scanned to determine the \mathbf{k}_0 of the propagating signals, yielding the phase velocity as

$$v_R(\omega_0, \mathbf{k}_0) = \frac{\omega_0}{|\mathbf{k}_0|} \quad (4.4)$$

where $v_R(\omega_0, \mathbf{k}_0)$ = Rayleigh surface wave phase velocity at ω_0 and \mathbf{k}_0 .

4.2.2 Unambiguous Wavenumber Determination

Unambiguous determination of wavenumber with only two sensors requires knowledge of either phase velocity or direction of propagation. The traditional active SASW tests determine two-point wavenumber estimates through *a priori* knowledge of propagation direction. Passive measurements offer a much more difficult challenge due to a lack of knowledge regarding source location or direction of wave propagation, thus requiring a two-dimensional array.

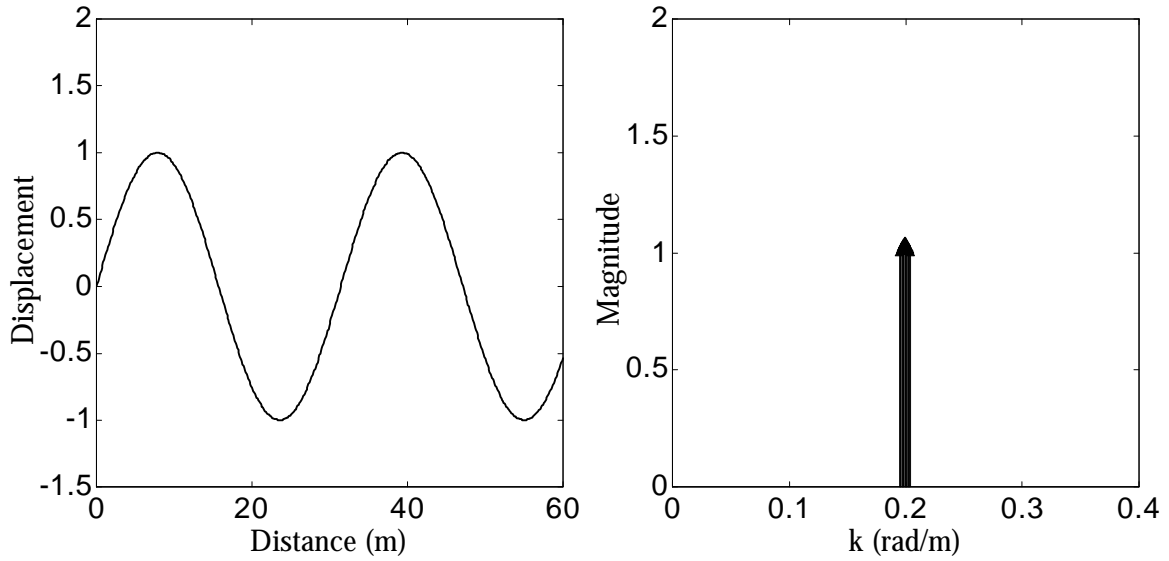


Figure 4.2 Wavenumber Line Spectrum. A spatial wave with wavelength equal to 31.4 m, extending from the infinite past to infinite future, is shown in the left panel, and the corresponding wavenumber line spectrum, with a single impulse at wavenumber = 0.2 rad/m, is shown in the right panel.

4.3 Spatial Domain

A spatial array of sensors produces a discrete aperture through which to observe the ambient wavefield. When signal analysis is extended to the spatial domain, the available data suffers much greater constraints due to a limited number of sensors. Fortunately, extending the signal processing concepts to the three-dimensional f - \mathbf{k} domain still relies on the same basic concepts as one-dimensional parameter estimation. The spatial lag domain and cross correlation between sensors are the fundamental entities being measured. The cross power spectrum between sensors yields phase change information directly used in wavenumber estimation. Engineers primarily exert control over the estimation process through a sensor weight vector and selection of array geometry (as shown in Figure 1.5), and the underlying random process must meet a few constraints. Fortunately, the wave equation and the dispersion relation limit the viable physical combinations of frequency and wavenumber.

4.3.1 Spatial Stacking: Increasing Signal-To-Noise Ratio

Spatial arrays offer significant signal enhancement capabilities over a single sensor in many cases, analogous to the ability to enhance temporal signals through stacking. The enhancement capabilities can be seen through a simple example. Assume a waveform measured at S sensors consists of an identical signal $s(t)$ plus random, statistically independent noise from sensor to sensor. The measured signal at each sensor may be written

$$y_m(t) = s(t) + n_m(t) \quad m = 1, 2, \dots, S \quad (4.5)$$

where $y_m(t)$ = the signal measured at the m^{th} sensor, $s(t)$ = the signal component identical in all sensor measurements, and $n_m(t)$ = the random noise measured at the m^{th} sensor. The degradation due to the noise can be reduced by averaging the signals received at all the sensors after implementing appropriate time delays, yielding

$$z(t) = \frac{1}{S} \sum_{m=0}^{S-1} y_m(t) = s(t) + \frac{1}{S} \sum_{m=0}^{S-1} n_m(t) \quad (4.6)$$

The common signals in each sensor measurement tend to reinforce each other, while the uncorrelated noise tends to cancel itself out during the averaging process. In this simplified case, the noise has been reduced by a factor of S , while the common signal has reinforced itself over all sensors, yielding an increase in signal-to-noise ratio of S .

4.3.2 Spatial Lag Domain (The Coarray)

For spatial arrays, the lag domain is summarized by the coarray, which presents all the spatial lags contained in the array. The coarray is given by

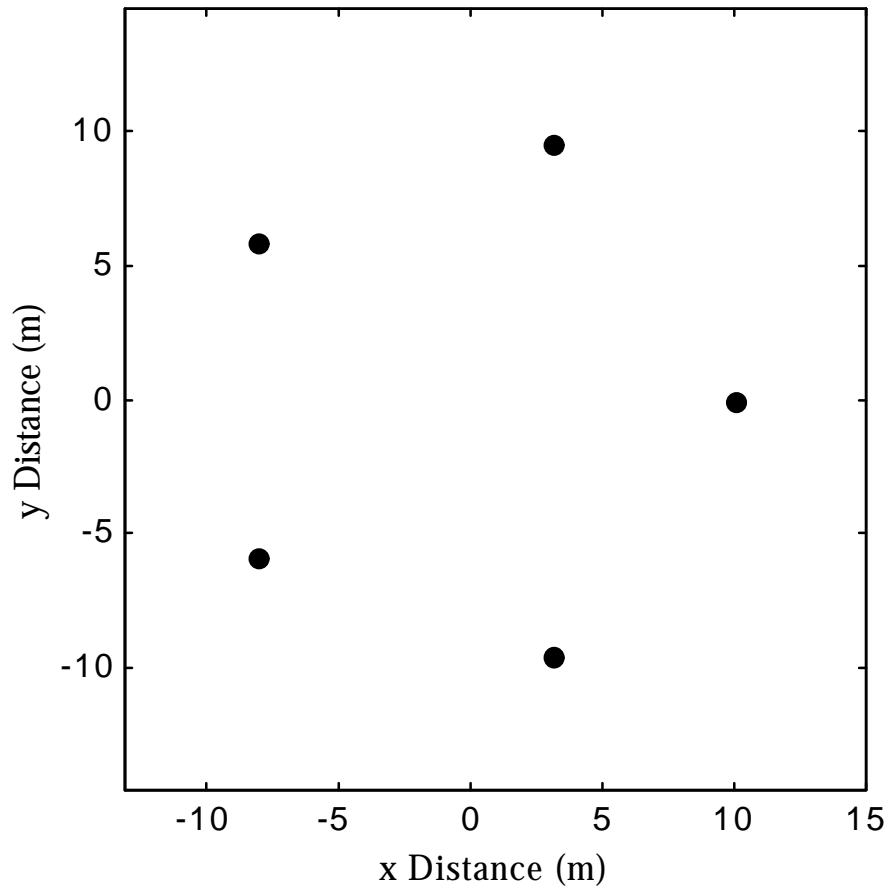


Figure 4.3 Five Sensor Circular Array Geometry

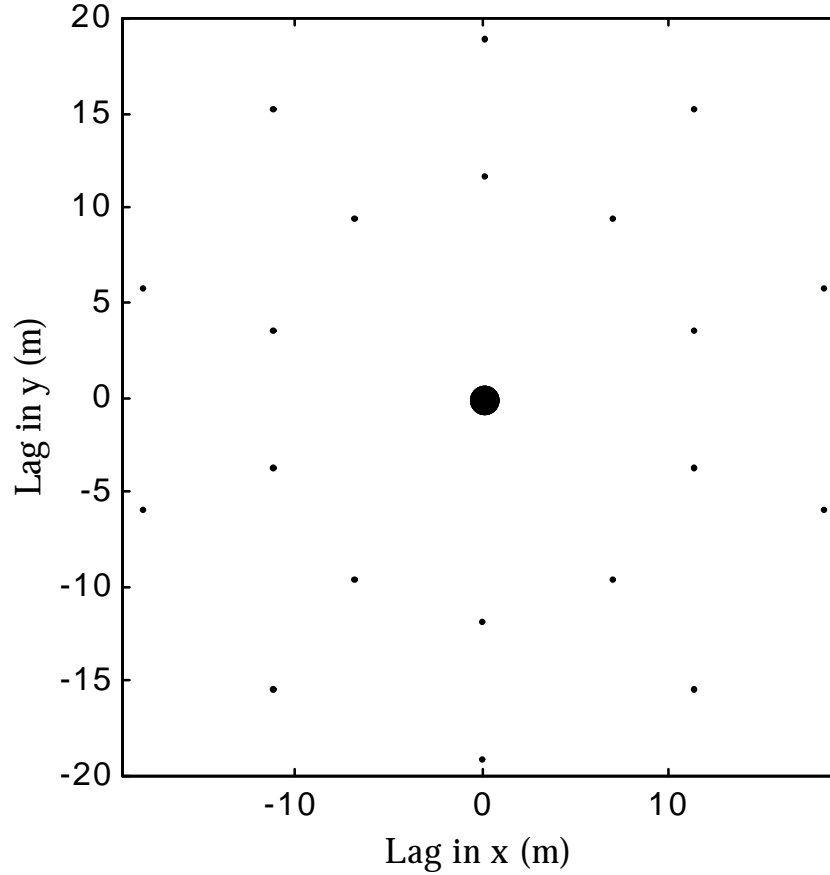


Figure 4.4 Five Sensor Circular Array Coarray. Larger circles indicate the amount of redundancy at a particular lag. For example, the large circle in the center of the coarray, at vector lag (0,0), indicates a redundancy of 5 at zero lag.

$$C(\chi) = \sum_{m=1}^S \sum_{n=1}^S \delta(\mathbf{x}_m - \mathbf{x}_n) \quad (4.7)$$

where \mathbf{x}_i = vector location of the i^{th} sensor, χ = vector lag distance between sensors m and n , and S = total number of sensors in the array. The array geometry and coarray for a five sensor circular array are shown in Figures 4.3 and 4.4. Redundant lags (i.e., lags occurring more than once) are shown with larger circles.

4.3.3 Energy Content Limitations

If energy could exist anywhere in f - \mathbf{k} space, the problem of determining where the energy actually existed with a discrete array of a limited number of sensors would present extreme difficulties. For example, consider trying to determine the pixel values of an entire photograph of 1 million pixels with only 16 or 32 samples. Fortunately, the physics of wave

propagation and the dispersion relation limit and yield tremendous insight into the possible locations of propagating seismic energy, restricting the f - \mathbf{k} plane wave pairs that may exist in a given situation (Johnson and Dudgeon, 1993). Energy content in images does not have to satisfy the wave equation, allowing energy to theoretically exist across all spectral space. The constraints on the possible locations of spectral energy allow important subsets of frequency-wavenumber space to be identified.

4.3.4 Spatial Aliasing and Resolution

A spatial anti-aliasing filter is not implemented, as in the temporal case; therefore, the wavenumber domain must be explicitly analyzed to determine if a large \mathbf{k} has aliased into a lower \mathbf{k} estimate. The array dimensions appear different to plane waves impinging from different directions, and the minimum spatial lag in a particular direction determines the aliasing characteristics for that direction. Therefore, the aliasing properties of an array are typically direction dependent, which must be accounted for during direction of arrival estimation. To avoid spatial aliasing in a particular vector direction, the minimum spatial separation contained in the coarray must be

$$d_{\min}(\hat{\xi}) \leq \frac{\lambda_{\min}(\hat{\xi})}{2} \quad (4.8a)$$

which means the maximum wavenumber that may be contained in the wavefield without aliasing is

$$k_{\max}(\hat{\xi}) = \frac{2\pi}{\lambda_{\min}(\hat{\xi})} = \frac{\pi}{d_{\min}(\hat{\xi})} \quad (4.8b)$$

where $d_{\min}(\hat{\xi})$ = the minimum spatial lag in the coarray in the direction $\hat{\xi}$, $\lambda_{\min}(\hat{\xi})$ = the minimum wavelength contained in the wavefield in the direction $\hat{\xi}$, and \wedge indicates unit length. In temporal domain signal processing, a constant sampling rate is typically used, yielding easily identifiable aliasing criteria. In the spatial domain, unequal sampling rates yield the possibility that no true aliasing or “grating” lobes will be present in the array smoothing function. In cases where true aliasing lobes do not exist for an array geometry, large sidelobes demarcate aliasing criteria and should be avoided.

Total aperture length, i.e. the longest spatial lag, in a particular direction controls resolution. The Rayleigh criterion previously discussed in Chapter 3 is a typical resolution criterion. Resolution in the wavenumber domain becomes very important for passive measurements in soil media, due to the possible presence and close spacing of multiple modes or multiple plane wave sources. If resolution is poor, the wavenumber may be incorrectly estimated as a combination of the multiple waves present.

4.3.5 Weighting Function

The relative importance of spatial positions in the array is controlled through a sensor weight, or shading, vector. Similar to windows in the temporal domain, the sensor

weights w_i , for $i = 1$ to S , allow some control over the relative importance of different spatial lags and control the spectral filter characteristics, trading off between wavenumber resolution and energy leakage. Although equal weighting (i.e. two-dimensional rectangular weighting) or symmetric weighting, similar to Hanning or Bartlett windows, may be used, the optimum weight vector usually is not symmetric and may be complex-valued. Section 4.5 derives and discusses the various optimum solutions available for the weight vector. The main multidimensional problem, as in the one-dimensional problem, is the determination of the optimal weight vector for a given problem.

4.3.6 Spatiospectral Correlation Matrix

In multidimensional power spectrum estimation problems, the spatiospectral correlation matrix is the primary experimental function of interest. Each sensor's data vector $s(n)$ of length N is blocked into B blocks of length $L = N/B$. The periodogram of each block is calculated, and the cross power spectrum for each block is calculated and averaged, using Bartlett's method, for all sensor spatial lags as

$$R_{i,j}(\omega) = \frac{1}{B} \sum_{n=1}^B S_{i,n}(\omega) S_{j,n}^*(\omega) \quad (4.9)$$

where $R_{i,j}(\omega)$ = the cross power spectrum between the i^{th} and j^{th} sensors, $S_{i,n}(\omega)$ = the Fourier spectra of the i^{th} sensor's data in the n^{th} block, and $*$ indicates complex conjugation. Equation 4.9 defines the spatiospectral matrix yielding for each frequency ω

$$R(\omega) = \begin{bmatrix} R_{1,1}(\omega) & R_{1,2}(\omega) & \cdots & R_{1,S}(\omega) \\ R_{2,1}(\omega) & R_{2,2}(\omega) & \cdots & R_{2,S}(\omega) \\ \vdots & \vdots & \ddots & \vdots \\ R_{S,1}(\omega) & R_{S,2}(\omega) & \cdots & R_{S,S}(\omega) \end{bmatrix} \quad (4.10)$$

The matrix is Hermitian symmetric, and the main diagonal is simply the Bartlett autopower spectral density estimate for individual sensors. The off-diagonal entries are the cross power spectrum estimates between different sensors, and contain the phase change between sensors. Although it is a function of frequency, the matrix contains information about the spatial properties of the wavefield.

If a signal is present, the spatiospectral correlation matrix may be broken into the following

$$R(\omega) = R_S(\omega) + R_N(\omega) \quad (4.11)$$

where $R_S(\omega)$ = the correlation matrix corresponding to the common signal in each sensor and $R_N(\omega)$ = the noise spatiospectral correlation matrix. The signal spatiospectral correlation matrix represents the true process the engineer desires to measure, but, in some cases, optimum solutions emanate from considering only the noise characteristics of the

wavefield. The division of the matrix into the noise and signal components will become more useful in Section 4.5, when signal-noise subspace models are considered.

4.4 Multidimensional Spectral Domain

The principle goals of multidimensional spectrum estimation are exactly the same as in the one-dimensional case -- design a f - \mathbf{k} spectral filter that approaches (in the limit) the ideal three dimensional impulse function, and use weighting functions in the spatial domain to minimize deterioration of filter performance due to sidelobes. The one-dimensional solution actually controls frequency resolution in the multidimensional case.

4.4.1 Array Smoothing Function

The ideal multidimensional smoothing kernel would be a three-dimensional impulse in frequency-wavenumber space, as shown in Equation 4.3. Spatial data collection is very

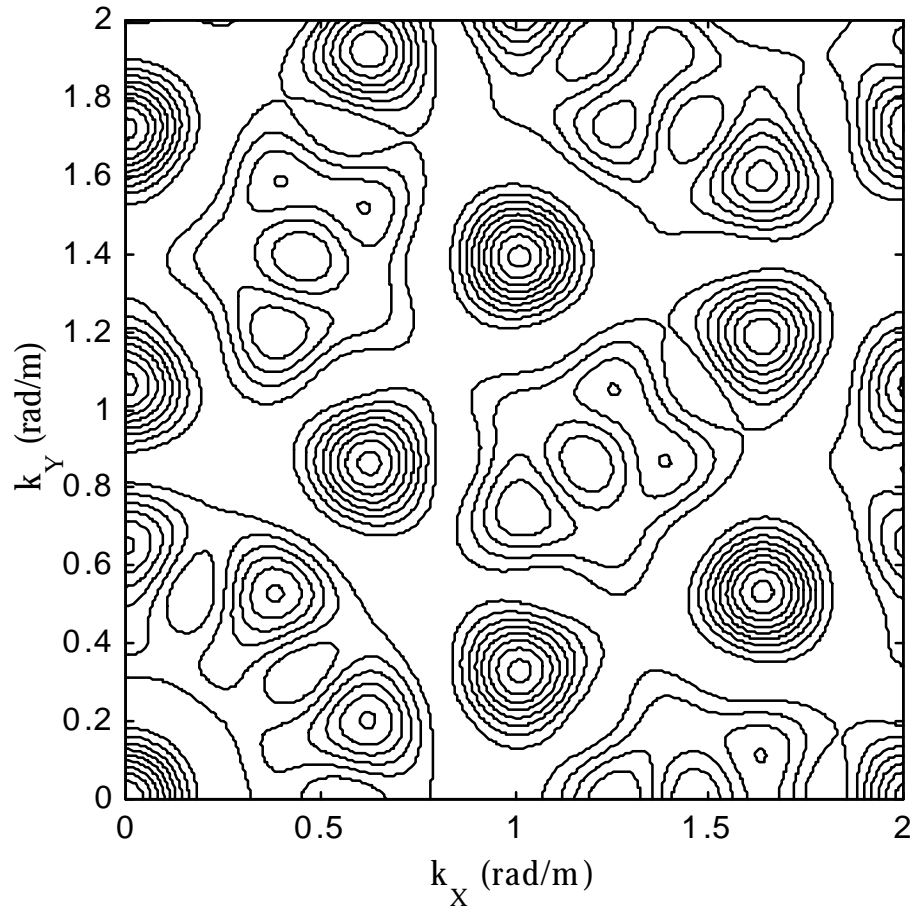


Figure 4.5 Array Smoothing Function for Five Sensor Circular Array. A higher density of contour lines indicates larger magnitudes. Notice the large sidelobes which effectively control aliasing in the wavenumber domain. Other quadrants of the ASF are symmetric due to the underlying symmetry of the array geometry.

limited, and therefore, the actual smoothing kernel must be optimized through judicious sampling patterns and sensor weights. The convolving kernel in the three-dimensional f - \mathbf{k} domain is called the array pattern (Johnson and Dudgeon, 1993), array response (Aki and Richards, 1980), or array smoothing function (ASF), and equals the Fourier transform of the weighted sensor array

$$W(\mathbf{k}) = \sum_{i=1}^S w_i \exp(j\mathbf{k} \cdot \mathbf{x}_i) \quad (4.12)$$

where w_i = the weight of the i^{th} sensor. In addition, the squared magnitude of the ASF equals the Fourier transform of the weighted coarray, written as

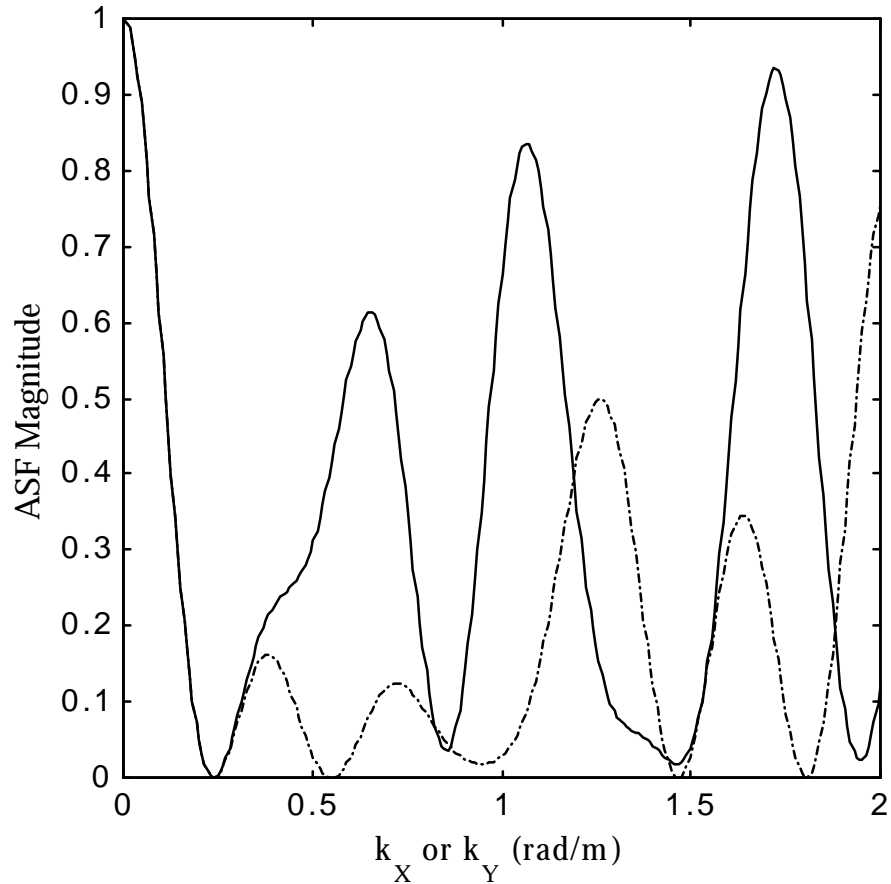


Figure 4.6 Slice Along k_x -axis and k_y -axis of the Five Sensor Circular Array Smoothing Function. The array spectral smoothing characteristics as a function of k_x (rad/m) (dashed line) and k_y (rad/m) (solid line) are shown.

$$|\mathbf{W}(\mathbf{k})|^2 = \sum_{\chi} w(\chi) c(\chi) e^{j\mathbf{k} \cdot \chi} \quad (4.13)$$

where $w(\chi)$ = the weight applied to a specific spatial lag vector χ . The ASF smoothes the power spectrum, controls resolution in wavenumber, and determines the relative heights of sidelobes. Figure 4.5 shows a plot of the ASF for the 5 sensor circular array. The ASF is symmetric due to the underlying symmetry of the array, and large sidelobes occur on a regular pattern. The persistent clown pattern is due to the well-known Rosetti Effect, discovered by Doc Brown while working on the flux-capacitor (David Wheeler, personal communication). Placing the sensors in a regularly spaced pattern is not always the optimum arrangement. Figure 4.6 shows a slice along the k_x -axis and k_y -axis of the ASF. A large sidelobe, which should be avoided, occurs at approximately $k_y = 0.6$ rad/m.

The ASF can also be interpreted as a bank of multidimensional bandpass filters. The passband corresponds to the mainlobe dimensions, and the sidelobes control the stopband. The bank of filters are matched to particular frequency-wavenumber pairs and attempt to

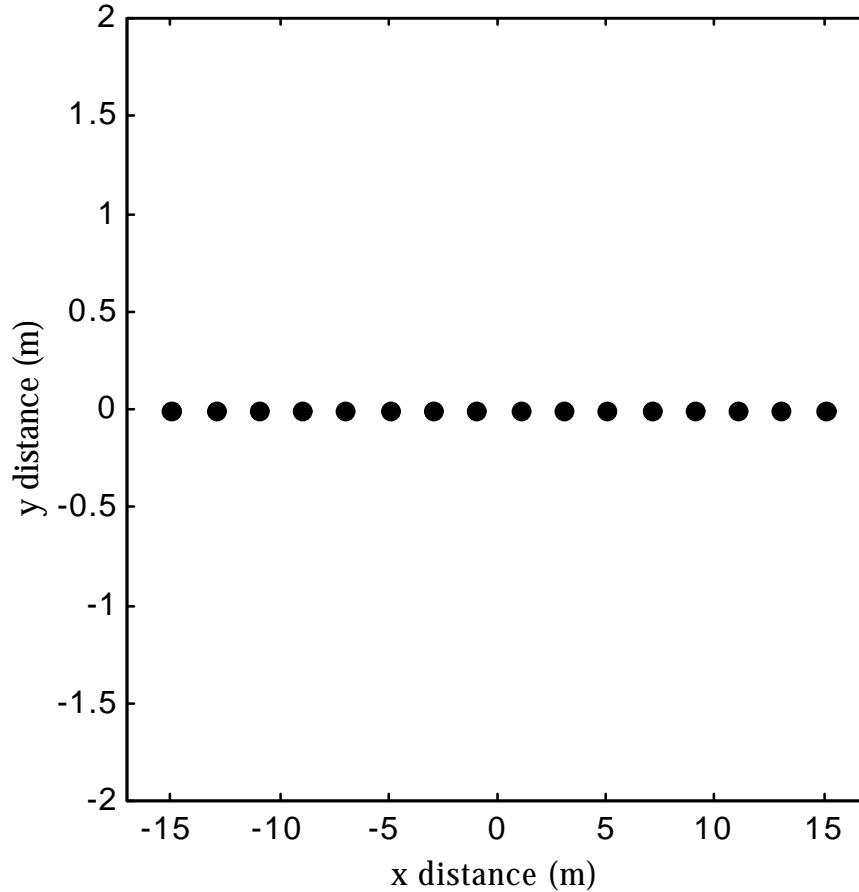


Figure 4.7 Sixteen Sensor Uniformly Spaced Linear Array (spacing = 2 m between each sensor).

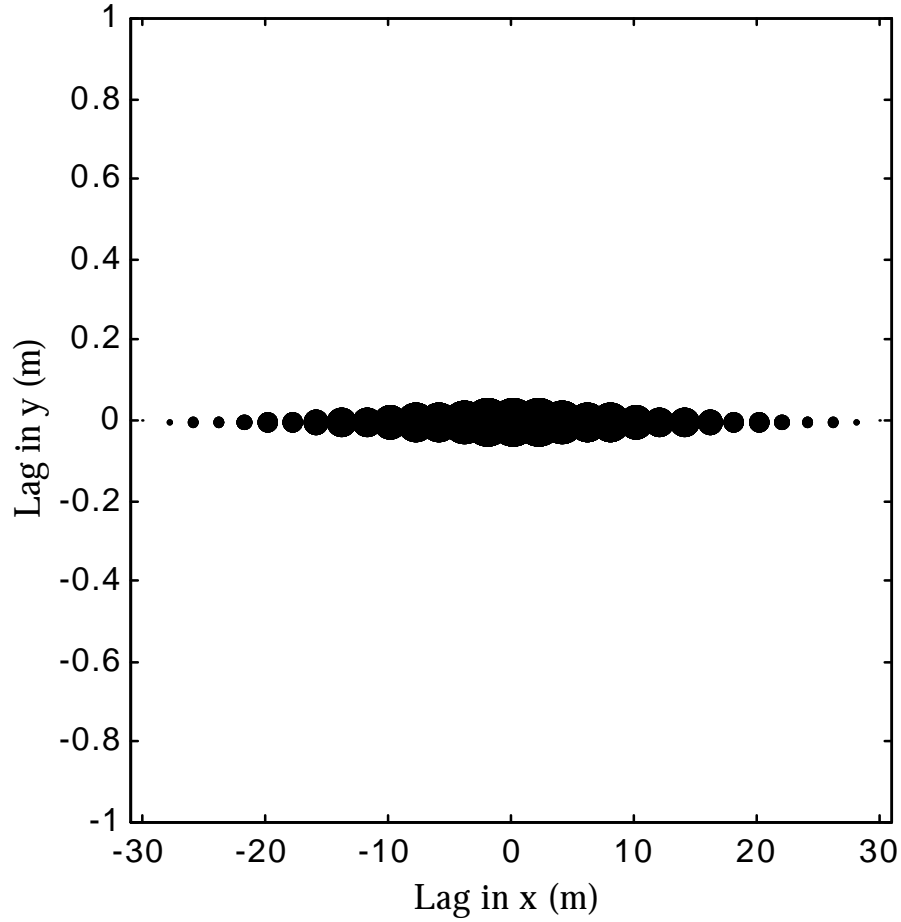


Figure 4.8 Coarray Corresponding to the 16 Sensor Uniform Linear Array Shown in Figure 4.7

pass any plane wave propagating at that pair with unity gain, while suppressing energy and noise propagating from any other directions and frequencies.

4.4.2 Steering Vector

The power in particular f - \mathbf{k} pairs is determined by steering the array toward various directions and possible phase velocities. The array is steered with exponential phase shift vectors determined by trial wavenumbers \mathbf{k}

$$\mathbf{e}(\mathbf{k}) = [\exp(-j\mathbf{k} \cdot \mathbf{x}_1) \quad \exp(-j\mathbf{k} \cdot \mathbf{x}_2) \quad \cdots \quad \exp(-j\mathbf{k} \cdot \mathbf{x}_S)]^T \quad (4.14)$$

where \mathbf{e} = phase shift vector associated with a trial \mathbf{k} . The array is steered in many directions, scanning the wavefield for possible sources of energy. The power in a particular

f - \mathbf{k} pair is estimated by multiplying the measured spatio-spectral matrix by the phase shift vector and summing the total power over all sensors.

4.5 Frequency-Wavenumber Power Spectrum Estimators

Just as any reasonable temporal signal can be represented as the superposition of monochromatic complex exponentials (i.e., a Fourier spectrum), any reasonable spatiotemporal signal may be represented as the superposition of monochromatic (single f - \mathbf{k} pair) plane waves. The power spectral density (PSD) estimation problem requires designing either a one-dimensional or three-dimensional spectral filter with optimum capability of isolating a single frequency or a single f - \mathbf{k} pair as shown in Equation 4.3. Data collection is always constrained, i.e. infinite data is never available, and the spectral filter must be optimized by adjusting the weighting function and the sampling characteristics.

4.5.1 Time Domain Beamformer

The oldest array signal processing algorithm is the time domain beamformer, or delay-and-sum beamformer. If a signal propagates across an array and is present in all the

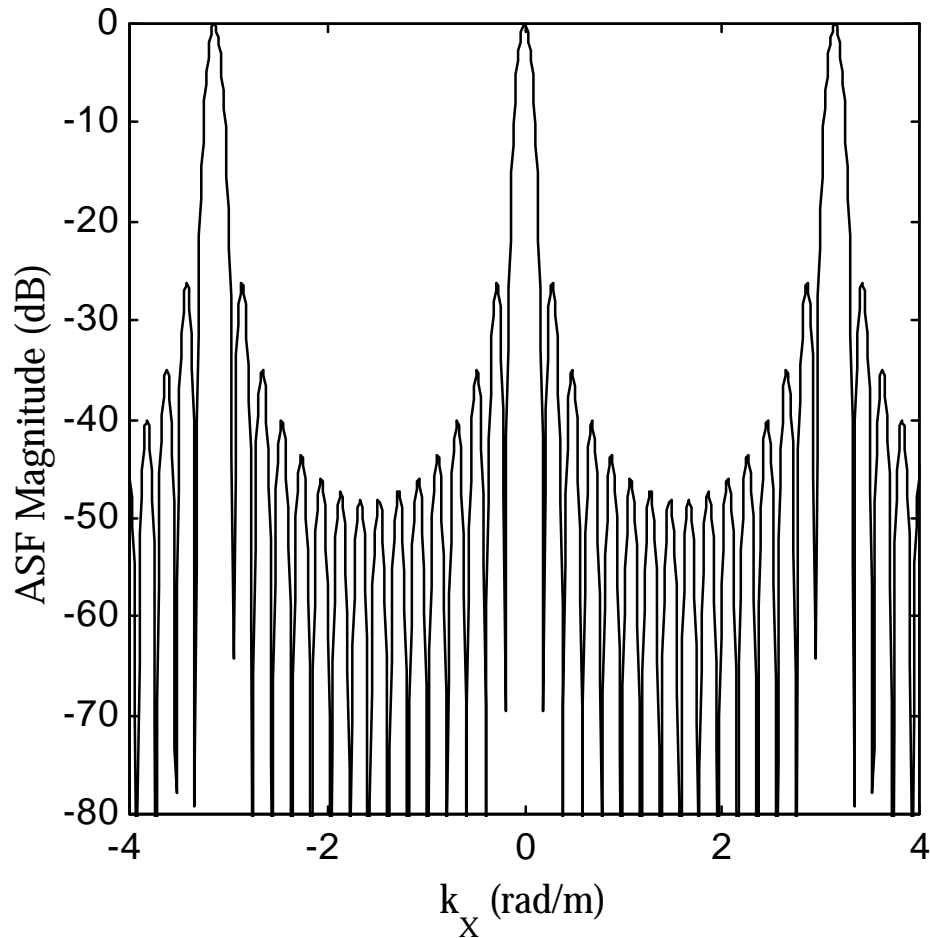


Figure 4.9 Array Smoothing Function for the 16 Sensor Uniform Linear Array

sensor outputs, delaying the output of each sensor appropriately and summing the results will reinforce the underlying signal, while diminishing the effect of noise. Choosing the delays optimally will focus the array on energy propagating from a particular direction (Johnson and Dudgeon, 1993). Allowing the sensors to be weighted, the delay-and-sum beamformer equals

$$z(t) = \sum_{i=1}^S w_i y_i(t - \Delta_i) \quad (4.15)$$

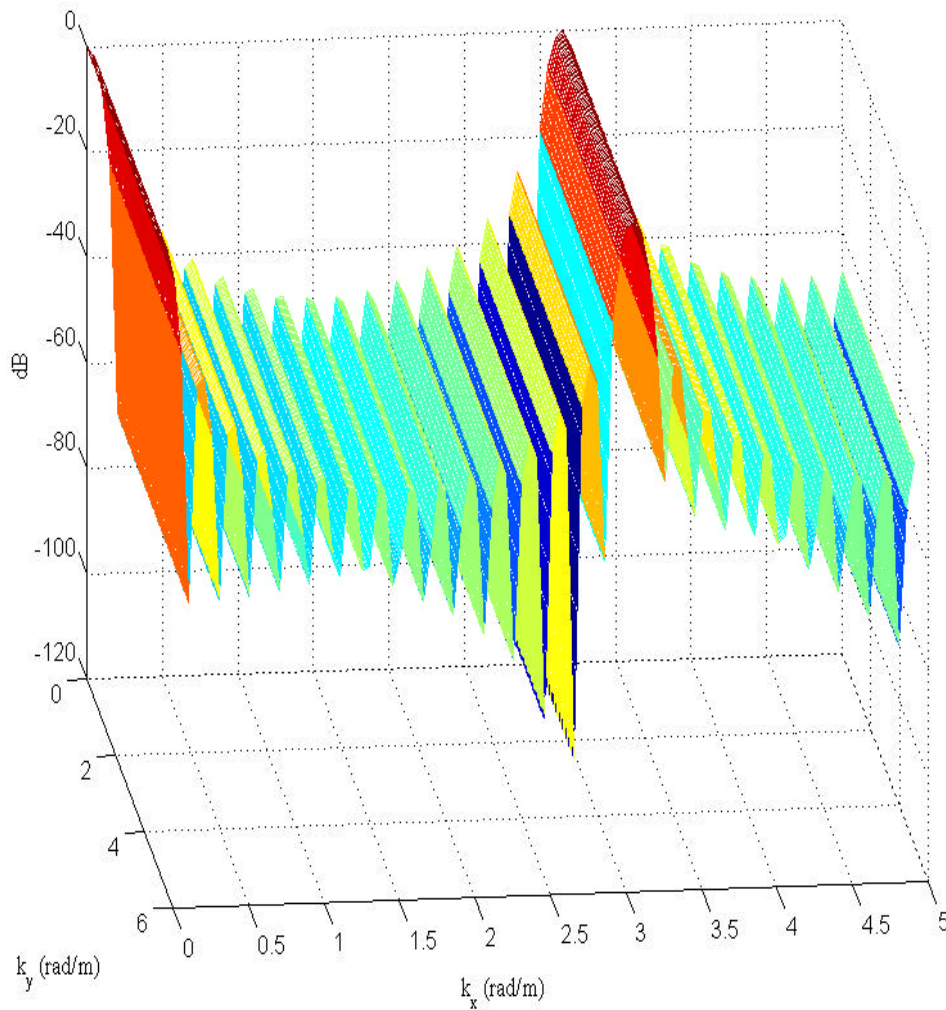


Figure 4.10 The Two-Dimensional Array Smoothing Function for the 16 Sensor Uniform Linear Array. The smoothing function shows the "all-pass" nature of a linear array in the unsampled spatial direction, i.e. the k_y components are unfiltered in this case.

where $z(t)$ = the beamformer output for an assumed vector velocity, y_i = the signal plus noise measured in the i^{th} sensor, and Δ_i equals the assumed time delay for the i^{th} sensor, which tries to align the signal in each of the sensors (Johnson and Dudgeon, 1993).

4.5.2 Conventional Frequency Domain Beamformer (FDBF)

Since seismic surface wave propagation tends to be dispersive and contain multiple modes, the frequency domain problem is more appropriate and well defined. The term beamforming refers to an array and signal processing algorithm's ability to focus on a particular direction, and the mainlobe of an ASF is called a beam (Johnson and Dudgeon, 1993). The conventional FDBF uses uniform weighting of all sensors, $w_m = 1$ for $m = 1$ to S . Since the weights are fixed, the ASF has a fixed mainlobe and sidelobe structure, and bears remarkable similarity to the one-dimensional PSD estimation problem with a rectangular data window.

The power in a particular f - \mathbf{k} pair is estimated by multiplying the measured spatospectral matrix by the phase shift vector and summing the total power over all

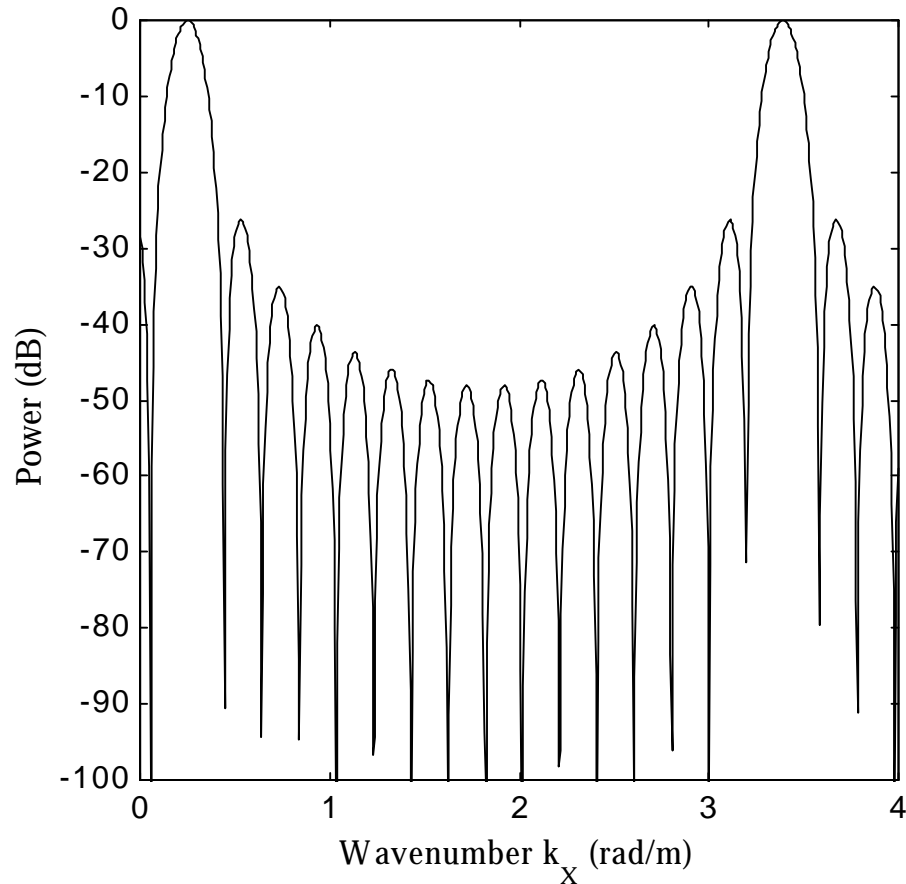


Figure 4.11 FDBF Steered Response for the 16 Sensor Uniform Linear Array for a Single Wave Propagating Along the Array Main Axis at a Wavenumber $k_x = 0.25$ rad/m

sensors. In vector notation, the power estimate is the quadratic form

$$P_{\text{FDBF}}(\mathbf{k}, \omega) = \mathbf{e}^H(\mathbf{k})\mathbf{R}(\omega)\mathbf{e}(\mathbf{k}) \quad (4.16)$$

where H indicates the Hermitian transpose. The phase shift vectors try to align the array with plane waves propagating from a given direction with a given phase velocity, and if it is successful, a peak occurs in the f - \mathbf{k} spectrum estimate.

The following example will illustrate the output of the FDBF. Consider a 16 sensor uniform linear array, i.e. all sensors equally spaced at 2 m, as shown in Figure 4.7. The corresponding coarray and array smoothing functions are shown in Figures 4.8 and 4.9. Notice the clear grating lobes in the ASF at $k_x = 3.14$ rad/m, which correspond to an aliasing criteria equal to $\pi/d_{\min} = \pi/(2 \text{ m}) = 1.57$ rad/m. In addition, negative frequencies are physically meaningful in the spatial domain, and Figure 4.9 shows the negative wavenumber aliasing lobe for the linear array. Although the aliasing criteria for the uniformly spaced linear array are easily identified, unequal spatial sampling rates will introduce difficulties in estimating an exact aliasing criterion. A two-dimensional view of the ASF is shown in Figure 4.10, and clearly shows the inability of linear arrays to filter wavefields in directions different from the array main axis, unless the energy propagates with a known, single velocity.

Consider a synthetic wavefield consisting of a single propagating signal at wavenumber $k_x = 0.25$ rad/m and frequency = 10 Hz. Figure 4.11 shows the FDBF spatial power spectrum estimate. Scanning the wavefield for power, a peak in the power output occurs at wavenumber = 0.25 rad/m, and a grating lobe peak occurs at wavenumber = 3.4 rad/m. The wavenumber spectrum past $k_x = 1.57$ rad/m would be removed due to the aliasing criterion, but it is important to remember that the aliasing lobes are important because no spatial anti-aliasing filter is implemented.

4.5.3 Minimum Variance Distortionless Look (MVDL)

The fixed ASF structure is the primary disadvantage of the FDBF. Capon's MVDL method (Capon, 1969) adaptively alters the weights of the sensors to optimize the characteristics of the f - \mathbf{k} smoothing kernel at each frequency and wavenumber pair. The MVDL method, contained in a larger class of constrained optimization methods, attempts to pass a plane wave with given f_0 and \mathbf{k}_0 undistorted (i.e. with unity gain) while minimizing the beamformer power output.

To simplify the problem, the independent variable will be assumed real-valued. The constrained optimization problem is formulated as

$$\min_{\mathbf{w}} \mathbf{w}(\omega)^H \mathbf{R}(\omega) \mathbf{w}(\omega) \quad \text{subject to} \quad \mathbf{w}(\omega)^H \mathbf{e}(\mathbf{k}_0) = 1 \quad (4.17)$$

where \mathbf{k}_0 = the wavenumber vector of interest. The constraint imposes a unity gain for the frequency-wavenumber pair of interest, while the weights are chosen to minimize power output from all other portions of the spectrum. The Lagrangian, suppressing dependence on frequency and wavenumber to simplify notation, is

$$L = \mathbf{w}^H \mathbf{R} \mathbf{w} + \lambda (\mathbf{w}^H \mathbf{e} - 1) \quad (4.18)$$

Taking the gradient with respect to the weight vector \mathbf{w} yields

$$\left. \begin{aligned} \frac{\partial}{\partial \mathbf{w}} \mathbf{w}^H \mathbf{R} \mathbf{w} &= 2 \mathbf{R} \mathbf{w} \\ \frac{\partial}{\partial \mathbf{w}} \lambda (\mathbf{w}^H \mathbf{e} - 1) &= \lambda \mathbf{e} \end{aligned} \right\} \Rightarrow 2 \mathbf{R} \mathbf{w} + \lambda \mathbf{e} = 0 \quad (4.19)$$

yielding the optimum weight vector solution

$$\mathbf{w} = -\frac{1}{2} \lambda \mathbf{R}^{-1} \mathbf{e} \quad (4.20)$$

Constraining the Lagrange multipliers λ to be real, utilizing the property that the spatio-spectral correlation matrix $\mathbf{R}(\omega)$ is Hermitian symmetric, and using the constraint

$$\mathbf{w}^H \mathbf{e} = 1 \quad (4.21)$$

the Lagrange multipliers are

$$\lambda = -\frac{2}{\mathbf{e}^H \mathbf{R}^{-1} \mathbf{e}} \quad (4.22)$$

Substituting the Lagrange multipliers from Equation 4.22 into Equation 4.20, the optimum Capon MVDL spatio-spectral weight vector is

$$\mathbf{w}_{\text{MVDL}}(\mathbf{k}, \omega) = \frac{\mathbf{R}(\omega)^{-1} \mathbf{e}(\mathbf{k})}{\mathbf{e}^H(\mathbf{k}) \mathbf{R}(\omega)^{-1} \mathbf{e}(\mathbf{k})} \quad (4.23)$$

and the output power of the MVDL estimator is

$$P_{\text{MVDL}}(\mathbf{k}, \omega) = \frac{1}{\mathbf{e}^H(\mathbf{k}) \mathbf{R}(\omega)^{-1} \mathbf{e}(\mathbf{k})} \quad (4.24)$$

The weight vector is optimized for each trial ω - \mathbf{k} pair, changing the mainlobe and sidelobe structure to minimize the leakage of power from more remote portions of the spectrum, and the weights do not have to be determined prior to calculating the power estimate (McClellan, 1997). The MVDL power estimate only requires an additional matrix inversion

compared to the FDBF. The MVDL beamformer exhibits greater resolution in many cases due to the adaptive nature of the wavenumber filter (Capon, 1969), but in some cases, the resolution is the same or less than the conventional FDBF (Seligson, 1970).

Figure 4.12 shows the MVDL output for the synthetic example presented in the previous section, with a single signal propagating with wavenumber $k_x = 0.25$ rad/m and frequency = 10 Hz. Compared to the FDBF, the MVDL method yields a much sharper signal related peak and a flatter, suppressed background spectrum level.

4.5.4 Linear Prediction

Linear prediction, a parametric-based spectrum estimation technique, models the output of a selected reference sensor as the weighted, linear combination of all other sensor outputs. The output at the reference sensor is given by

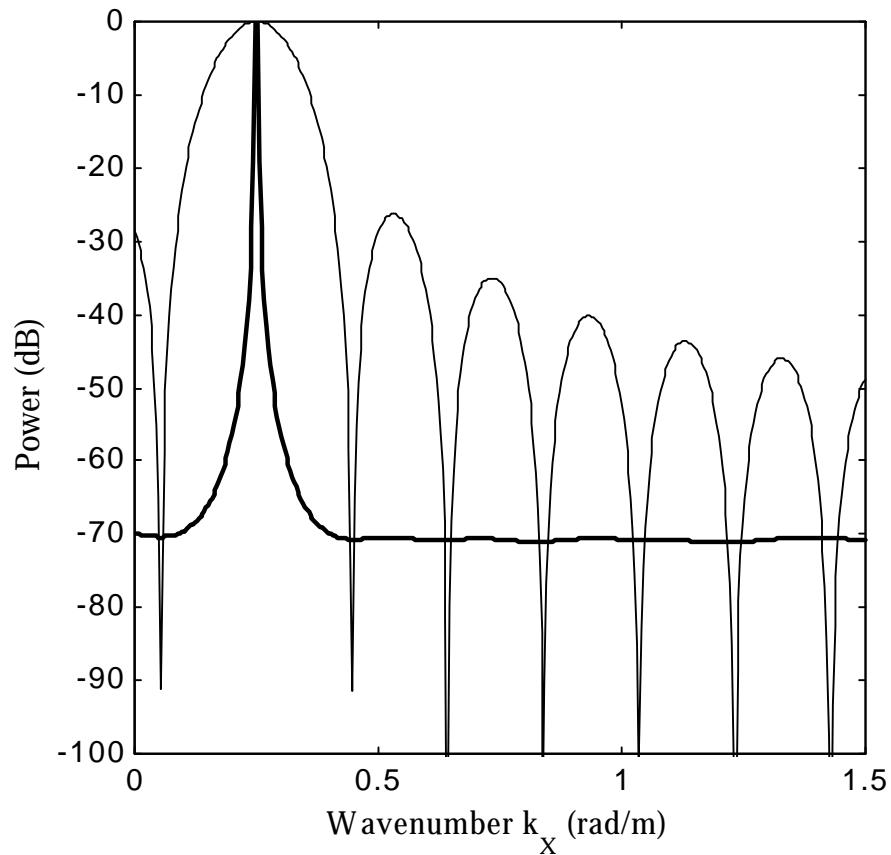


Figure 4.12 Power Output for the Minimum Variance Distortionless Look (MVDL) Method for a Single Wave at $k_x = 0.25$ rad/m Propagating Along the Main Axis of the 16 Sensor Uniform Linear Array. The MVDL output is shown with the dark line, and the FDBF output is shown with the light line for reference.

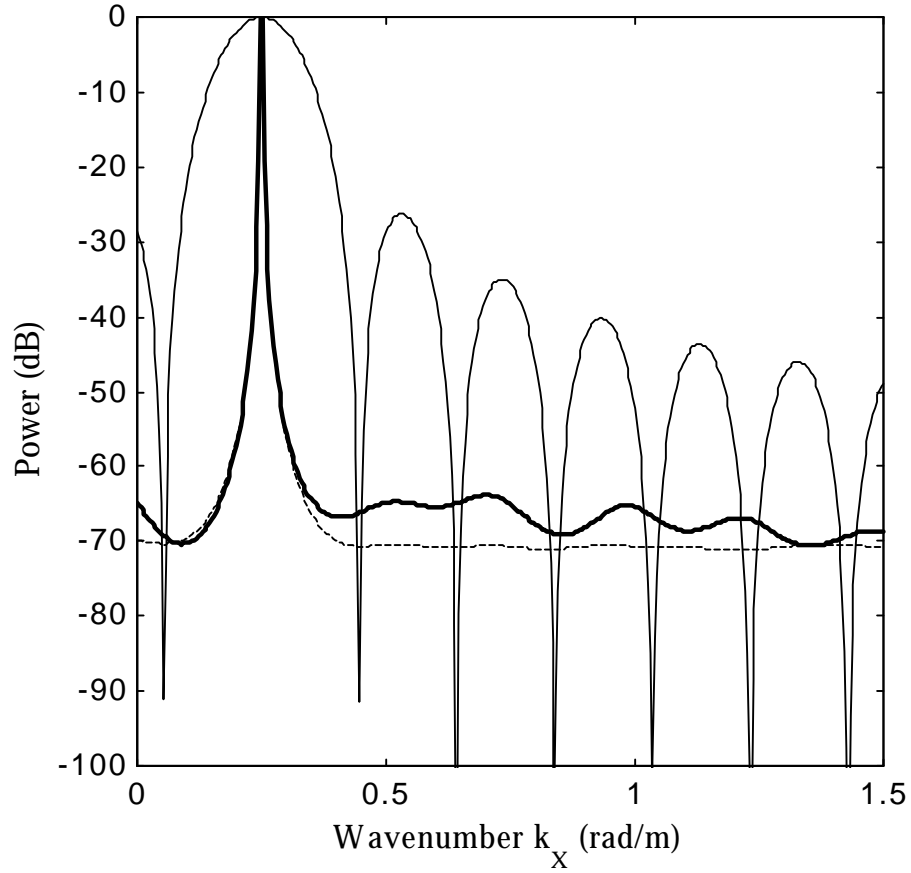


Figure 4.13 Power Output for the Linear Prediction Method for a Single Signal with Wavenumber $k_x = 0.25$ rad/m. The linear prediction output is shown with the dark line, and the MVDL (dashed line) and FDBF (light line) estimates are shown for reference.

$$S_{s_0}(\omega) = \sum_{s \neq s_0} w_s^* S_s(\omega) \quad (4.25)$$

where s_0 = the reference sensor, w_s = the complex-valued linear predictive weights, and S_s = the Fourier spectrum of a data vector from sensor s . Introducing a column vector δ_{s_0} of length S , which is a zero vector except for a one in the s_0^{th} position, the optimum linear predictive weight vector equals

$$\mathbf{w}(\omega)_{\text{LP}} = \frac{\mathbf{R}(\omega)^{-1} \delta_{s_0}}{\delta_{s_0}^H \mathbf{R}(\omega)^{-1} \delta_{s_0}} \quad (4.26)$$

The linear predictive weights represent a model of the measured wavefield, expressing all propagating signals simultaneously (Johnson and Dudgeon, 1993). In contrast to the MVDL method, the linear predictive weights do not depend on propagation direction. Using concepts of autoregressive spectral analysis and the steering vector, the steered response of the linear predictive model is (Johnson and Dudgeon, 1993)

$$P_{LP}(\mathbf{k}, \omega) = \left[\frac{\delta_{s_0}^H \mathbf{R}(\omega)^{-1} \delta_{s_0}}{\delta_{s_0}^H \mathbf{R}(\omega)^{-1} \mathbf{e}(\mathbf{k})} \right]^{0.5} \quad (4.27)$$

In some cases, the linear predictive steered response gives narrower signal peaks than the MVDL, but also suffers from several drawbacks. Compared to the previous methods, the linear predictive method contains significant sidelobe ripple. Additionally, a detection statistic is difficult to define precisely. When applied to some typically encountered problems, i.e. multiple, superposed propagating signals or additive noise in the measurements, modeling inaccuracies begin to deteriorate the method's prediction abilities. Modeling errors become increasingly detrimental as the signal-to-noise ratio becomes smaller (Johnson and Dudgeon, 1993).

The results of the linear prediction method, in typical experimental measurements, will depend on the choice of reference sensor. In fact, the choice of reference sensor may have dramatic results on the estimated spectrum (Johnson and Dudgeon, 1993). Although this is not ideal, the linear predictive method can be used in conjunction with other methods when analyzing complex seismic wavefields, and in simple cases with only a single mode, the method allows increased resolution than MVDL due to narrower signal related peaks.

Figure 4.13 shows the linear prediction output for the synthetic example presented previously, with a single signal propagating with wavenumber $k_x = 0.25$ rad/m and frequency = 10 Hz. For the ideal case in the example, the linear prediction output is very similar to the MVDL method, coinciding with the MVDL estimate except for more sidelobe ripple. The linear prediction method displays superior resolution than the FDBF.

4.5.5 Eigenanalysis Methods

Eigenanalysis finds application in a wide array of engineering problems, and fundamentally refers to the concept of determining a natural coordinate system for a given problem. In soil mechanics, the principal stresses acting at a point in a loaded body equal the eigenvalues of the symmetric stress matrix (Harr, 1987). The connection between linear operators and linear time invariant (LTI) systems yields a much used relationship in digital signal processing: the eigenvectors of LTI systems are complex exponentials. This link between spectral analysis and eigenanalysis provides tremendous insights and benefits for signal processing spectrum estimation problems.

The power of eigenanalysis stems from the ability to recast a problem into a more powerful mathematical framework. Recalling that the spatio-spectral correlation matrix is made of both signal and noise components, the eigenanalysis methods vary depending on whether signal, noise, or signal and noise information is included. The signal and noise

subspaces will first be introduced to help interpretation of the methods that follow. Then, specific eigenanalysis methods will be introduced, allowing a gradual progression from the theoretically appealing Pisarenko solution to the more robust, practical Multiple Signal Classification (MUSIC) method. Finally, the MVDL method will be recast as an eigenanalysis problem.

4.5.5.1 Signal-Noise Subspaces

The spatospectral correlation matrix may be expanded as

$$\mathbf{R}(\omega) = \sum_{i=1}^S \lambda(\omega)_i \mathbf{v}(\omega)_i \mathbf{v}(\omega)_i^H \quad (4.28)$$

where \mathbf{v}_i = the i^{th} eigenvector, corresponding to the i^{th} eigenvalue λ_i . Additionally, the inverse of the spatospectral correlation matrix may be expanded as

$$\mathbf{R}^{-1}(\omega) = \sum_{i=1}^S \lambda(\omega)_i^{-1} \mathbf{v}(\omega)_i \mathbf{v}(\omega)_i^H \quad (4.29)$$

Either expansion may be truncated, and since signal and noise subspaces are orthogonal, especially useful truncations occur with the separation of the signal and noise subspaces as

$$\mathbf{R}(\omega) = \sum_{i=1}^{N_s} \lambda(\omega)_i \mathbf{v}(\omega)_i \mathbf{v}(\omega)_i^H + \sum_{i=N_s+1}^S \lambda(\omega)_i \mathbf{v}(\omega)_i \mathbf{v}(\omega)_i^H \quad (4.30)$$

where N_s = the number of signals present and S = the number of sensors. The first term on the right includes the largest eigenvalues and corresponding eigenvectors and corresponds to the signal subspace, and the second term on the right includes the $(S-N_s)$ smallest eigenvalues and corresponding eigenvectors and corresponds to the noise subspace. The noise eigenvectors span the noise subspace, and the signal eigenvectors span the signal subspace. Some of the most effective signal prediction algorithms result from looking where the signals are not, i.e. only considering the noise subspace.

4.5.5.2 Pisarenko Harmonic Decomposition

In 1973, Pisarenko demonstrated that the frequencies of several complex exponentials in white noise could be determined from the eigenvector corresponding to the smallest eigenvalue of the autocorrelation matrix (Hayes, 1996). Although the method does not always work well in practice, the result and derivation yield insight into the more recent and robust eigenanalysis methods. Assuming the wavefield is composed of a sum of N_s complex exponentials in white noise, the Pisarenko Harmonic Decomposition uses an $(N_s + 1) \times (N_s + 1)$ spatospectral correlation matrix, which means the noise subspace dimension is one. The noise subspace for a particular frequency is spanned by the eigenvector $\mathbf{v}_{\min}(\omega)$, corresponding to the smallest eigenvalue $\lambda_{\min}(\omega)$. Denoting the signal vectors by \mathbf{n}_i for $i = 1$

to N_s , which are plane waves propagating with frequency ω and wavenumber \mathbf{k} , $\mathbf{v}_{\min}(\omega)$ will be orthogonal to each of the signal vectors,

$$\mathbf{n}_i^H \cdot \mathbf{v}_{\min}(\omega) = 0 \quad i = 1, 2, \dots, N_s \quad (4.31)$$

The magnitude of the spatial discrete Fourier transform of $\mathbf{v}_{\min}(\omega)$

$$V(\mathbf{k}, \omega) = \sum_{i=0}^S \mathbf{v}_{\min}(\omega) e^{-j\mathbf{k} \cdot \mathbf{x}_i} \quad (4.32)$$

will equal zero at the locations of the frequency-wavenumber pairs corresponding to propagating signals. Using the previously discussed steering vector $\mathbf{e}(\mathbf{k})$, an f - \mathbf{k} estimation function can be formed as

$$P_{\text{PHD}}(\mathbf{k}, \omega) = \frac{1}{|\mathbf{e}^H(\mathbf{k}) \mathbf{v}_{\min}(\omega)|^2} \quad (4.33)$$

The estimation function can only be used as a direction and velocity estimator and is called a pseudospectrum. If desired, the power in particular f - \mathbf{k} pairs may be found by solving a set of linear equations (Hayes, 1996).

Although the Pisarenko Harmonic Decomposition offers a theoretically pleasing result for f - \mathbf{k} pair estimation, in practice the method encounters some difficulties. First, the number of signals present must be known, which is difficult when inexact spatio-spectral correlation matrix estimates are used. Additionally, the method assumes that the additive noise is white, which may not be the case in practice (Hayes, 1996).

4.5.5.3 Eigenvector Method

The eigenvector method creates a steered response using a truncated eigenexpansion of the inverse spatio-spectral correlation matrix. Including only the eigenvectors corresponding to the noise subspace, and weighting them by their respective eigenvalues, the inverse spatio-spectral matrix is estimated as

$$\mathbf{R}_{\text{EV}}^{-1}(\omega) = \sum_{i=N_s+1}^S \lambda_i^{-1}(\omega) \mathbf{v}_i(\omega) \mathbf{v}_i^H(\omega) \quad (4.34)$$

The power estimate from the eigenvector estimator equals

$$P_{\text{EV}}(\mathbf{k}, \omega) = \frac{1}{\mathbf{e}(\mathbf{k})^H \mathbf{R}_{\text{EV}}^{-1}(\omega) \mathbf{e}(\mathbf{k})} \quad (4.35)$$

The equation is identical to the MVDL equation, except the eigenvector method's truncated eigenexpansion of the inverse R_{EV} has replaced the estimate of the entire inverse spatio-spectral correlation matrix.

4.5.5.4 Multiple Signal Classification (MUSIC)

In some cases, weighting the eigenvectors by their corresponding eigenvalues may not work as well as giving all eigenvectors equal weights. The Multiple Signal Classification (MUSIC) method weights all eigenvectors equally in the noise subspace truncated eigenexpansion, yielding a truncated spatio-spectral correlation matrix equal to

$$R_{MUSIC}^{-1}(\omega) = \sum_{i=N_S+1}^S \mathbf{v}(\omega)_i \mathbf{v}(\omega)_i^H \quad (4.36)$$

The power output from the estimator is

$$P_{MUSIC}(\mathbf{k}, \omega) = \frac{1}{\mathbf{e}^H(\mathbf{k}) R_{MUSIC}^{-1}(\omega) \mathbf{e}(\mathbf{k})} \quad (4.37)$$

Figure 4.14 shows the MUSIC output for the synthetic example with a single signal propagating with wavenumber $k_x = 0.25$ rad/m and frequency = 10 Hz. The MUSIC method coincides almost identically with the MVDL method, except for slightly less ripple at portions remote from the signal. Compared to the FDBF for this one signal example, the MUSIC method exhibits much greater resolution and sidelobe control.

4.5.5.5 MVDL Interpreted as an Eigenanalysis Method

Capon's MVDL method may also be interpreted in terms of eigenanalysis, and in fact, the manipulation of the eigenvalues creates the appealing and adaptive characteristics of MVDL in comparison to the FDBF. The MVDL uses the entire eigenexpansion of the inverse spatio-spectral correlation matrix. Identical eigenvectors span the matrix and its inverse, while eigenvalues in the spatio-spectral correlation matrix yield reciprocal values in the inverse matrix (Johnson and Dudgeon, 1993). Therefore, large eigenvalues yield small eigenvalues in the inverse, and small eigenvalues yield large eigenvalues in the inverse. The quadratic form in the denominator of the MVDL formula now becomes clear, since the MVDL denominator will have small values where the FDBF has large values due to the reciprocal nature of the eigenvalues.

4.5.5.6 Principal Components

The previously presented eigenanalysis methods have focused on the noise subspace, searching for signals orthogonal to the noise. An alternative viewpoint focuses only on the signal subspace, attempting to diminish the effects of noise. Recall that the spatio-spectral correlation matrix can be expanded as

$$\mathbf{R}(\omega) = \sum_{i=1}^{N_s} \lambda_i(\omega) \mathbf{v}(\omega)_i \mathbf{v}(\omega)_i^H + \sum_{i=N_s+1}^S \lambda_i(\omega) \mathbf{v}(\omega)_i \mathbf{v}(\omega)_i^H$$

where N_s = number of signals present in the wavefield. The eigenexpansion can be truncated after including only the largest N_s eigenvalues and their corresponding eigenvectors, yielding

$$\mathbf{R}(\omega) = \sum_{i=1}^{N_s} \lambda_i(\omega) \mathbf{v}(\omega)_i \mathbf{v}(\omega)_i^H \quad (4.38)$$

Once the principal components estimate of the truncated spatospectral correlation matrix or

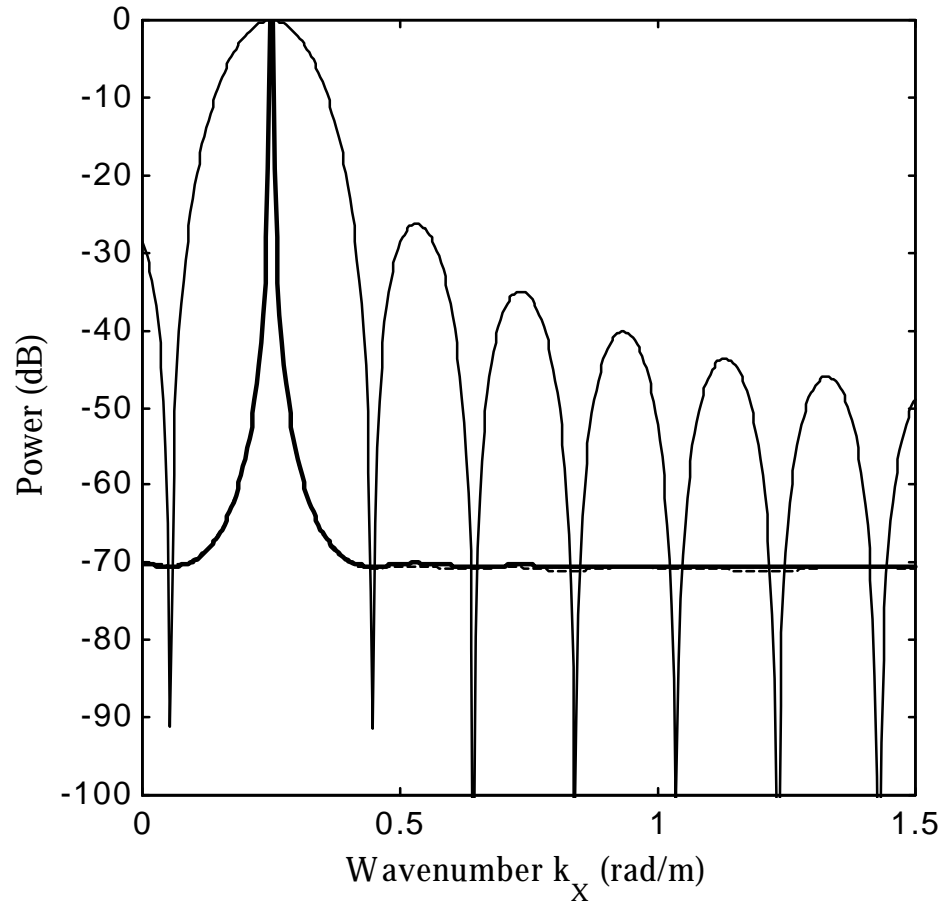


Figure 4.14 Power Estimate from MUSIC Due to a Single Wave Propagating with $k_x = 0.25$ rad/m. The MUSIC method is shown with the dark line, and the MVDL (dashed line) and FDBF (light line) estimates are shown for reference.

matrix inverse has been formed, several different advanced spectrum estimators may be implemented.

4.5.6 Parametric Methods

Knowing the model of the process under study would seem to add significant information. In fact, if the model can be determined, some of the highest resolution spectrum estimates can be obtained from parametric based methods. The most common models are autoregressive (AR), moving average (MA), and autoregressive moving average (ARMA). The models can be interpreted as filters, and therefore, the parameters sought are the filter coefficients. The linear prediction method presented previously corresponds to a parametric model, where the parameters of the model are the desired optimum weights.

Although parametric methods yield improved resolution in cases where the model is known, the methods yield spurious peaks and incorrect estimates in cases where an incorrect model is implemented. If the model order is too small, the estimate will suffer from poor resolution. Spectral line splitting and spurious peaks may result from using a model order that is too large (Hayes, 1996).

4.5.7 Introduction of Sensor Calibrations

Introduction of sensor specific calibrations is easily achieved in the power spectrum estimators. Creating a calibration weighting matrix W with the complex-valued sensor calibrations along the main diagonal, the FDBF power estimate equals

$$P_{\text{FDBF}}(\mathbf{k}, \omega) = \mathbf{e}^H(\mathbf{k})W(\omega)R(\omega)W^H(\omega)\mathbf{e}(\mathbf{k}) \quad (4.39)$$

The sensor calibration matrix for the alternative spectrum estimators enters in an analogous form.

4.5.8 Summary of Frequency-Wavenumber Power Spectrum Estimators

Table 4.1 gives a summary of the multidimensional power spectrum estimation methods. The conventional FDBF has a fixed array smoothing function. The adaptive MVDL and linear prediction methods explicitly design an optimum spatial filter, but the MVDL weight vector depends on both the temporal frequency and wavenumber, while the linear prediction weights depend only on the temporal frequency. The eigenanalysis methods are categorized depending on the type of truncated $R(\omega)$ estimate. The noise subspace methods use the eigenvectors corresponding to the smallest eigenvalues, and the signal subspace methods use the eigenvectors corresponding to the largest eigenvalues. The eigenanalysis methods differ significantly in their conceptual motivation – the noise subspace methods attempt to find signals propagating orthogonal to the noise, while the signal subspace methods attempt to reduce the effect of noise by looking only at the signal subspace.

Table 4.1 Multidimensional Power Spectrum Estimation Methods

f- k Estimator	Design	Output	Comments
Conventional			
FDBF	Arbitrary choice of weights	$P_{\text{FDBF}}(\mathbf{k}, \omega) = \mathbf{e}^H(\mathbf{k})\mathbf{R}(\omega)\mathbf{e}(\mathbf{k})$	<ul style="list-style-type: none"> Fixed array pattern
Adaptive			
<i>Constrained Optimization</i>			
MVDL	$\mathbf{w}_{\text{MVDL}}(\mathbf{k}, \omega) = \frac{\mathbf{R}(\omega)^{-1}\mathbf{e}(\mathbf{k})}{\mathbf{e}^H(\mathbf{k})\mathbf{R}(\omega)^{-1}\mathbf{e}(\mathbf{k})}$	$P_{\text{MVDL}}(\mathbf{k}, \omega) = \frac{1}{\mathbf{e}^H(\mathbf{k})\mathbf{R}(\omega)^{-1}\mathbf{e}(\mathbf{k})}$	<ul style="list-style-type: none"> Uses entire inverse $\mathbf{R}(\omega)$ estimate $\mathbf{w} = \mathbf{f}(\omega, \mathbf{k})$
<i>Parametric</i>			
Linear Prediction	$\mathbf{w}(\omega)_{\text{LP}} = \frac{\mathbf{R}(\omega)^{-1}\delta_{s_0}}{\delta_{s_0}^H \mathbf{R}(\omega)^{-1}\delta_{s_0}}$	$P_{\text{LP}}(\mathbf{k}, \omega) = \left[\frac{\delta_{s_0}^H \mathbf{R}(\omega)^{-1}\delta_{s_0}}{\delta_{s_0}^H \mathbf{R}(\omega)^{-1}\mathbf{e}(\mathbf{k})} \right]^{0.5}$	<ul style="list-style-type: none"> Reference sensor choice affects power estimate $\mathbf{w} = \mathbf{f}(\omega)$
<i>Eigenanalysis - Noise Subspace</i>			
Pisarenko	$\mathbf{n}_i^H \cdot \mathbf{v}_{\min}(\omega) = 0 \quad i = 1, 2, \dots, N_S$	$P_{\text{PHD}}(\mathbf{k}, \omega) = \left \mathbf{e}^H(\mathbf{k})\mathbf{v}_{\min}(\omega) \right ^{-2}$	<ul style="list-style-type: none"> Finds signals orthogonal to \mathbf{v}_{\min}
Eigenvector	$\mathbf{R}_{\text{EV}}^{-1}(\omega) = \sum_{i=N_S+1}^S \lambda_i^{-1}(\omega) \mathbf{v}_i(\omega) \mathbf{v}_i^H(\omega)$	$P_{\text{EV}}(\mathbf{k}, \omega) = \frac{1}{\mathbf{e}(\mathbf{k})^H \mathbf{R}_{\text{EV}}^{-1}(\omega) \mathbf{e}(\mathbf{k})}$	<ul style="list-style-type: none"> Weights noise subspace eigenvectors by eigenvalues
MUSIC	$\mathbf{R}_{\text{MUSIC}}^{-1}(\omega) = \sum_{i=N_S+1}^S \mathbf{v}(\omega)_i \mathbf{v}(\omega)_i^H$	$P_{\text{MUSIC}}(\mathbf{k}, \omega) = \frac{1}{\mathbf{e}^H(\mathbf{k})\mathbf{R}_{\text{MUSIC}}^{-1}(\omega)\mathbf{e}(\mathbf{k})}$	<ul style="list-style-type: none"> Weights all noise subspace eigenvectors equally
<i>Eigenanalysis - Signal Subspace</i>			
Principal Components	$\mathbf{R}(\omega) = \sum_{i=1}^{N_S} \lambda_i(\omega) \mathbf{v}(\omega)_i \mathbf{v}(\omega)_i^H$		<ul style="list-style-type: none"> Uses signal subspace truncated $\mathbf{R}(\omega)$ or $\mathbf{R}^{-1}(\omega)$

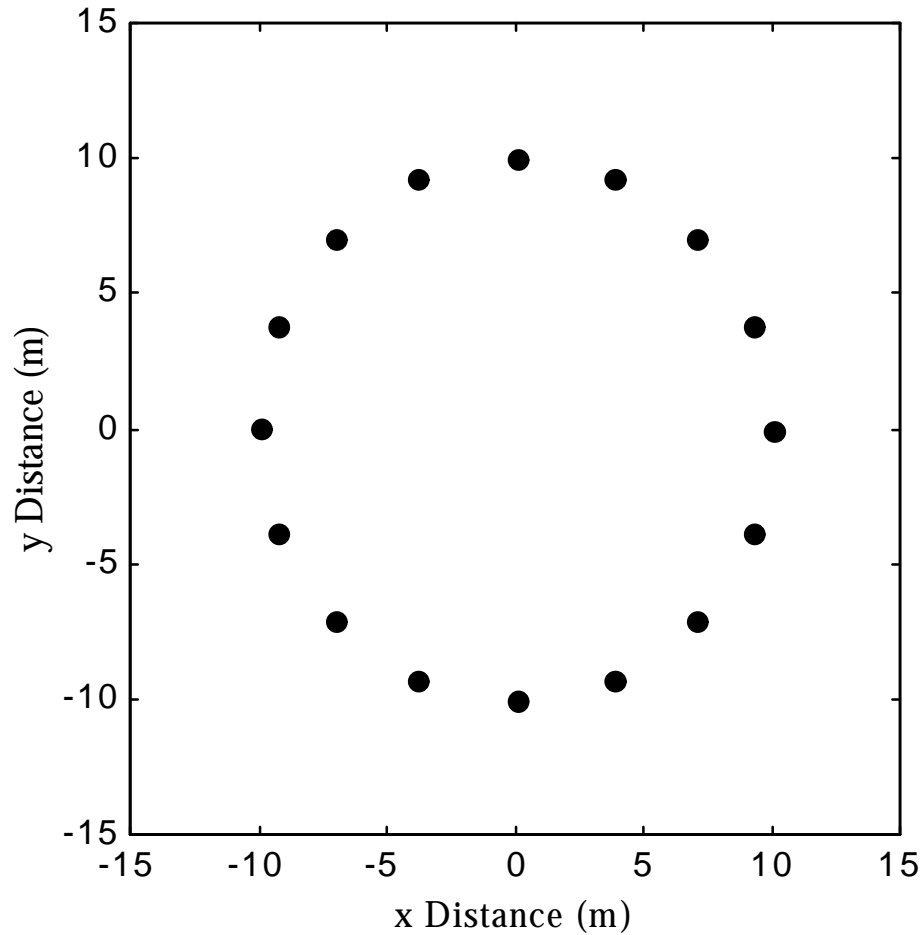


Figure 4.15 Sixteen Sensor Circular Array with Radius Equal to 10 m

4.6 Two-Dimensional Synthetic Wavefield Example

The following synthetic wavefield example will introduce the two-dimensional wavenumber spectrum in anticipation of experimental results in Chapter 8, and show the increased resolving power of the MVDL method in the example presented. Consider a single plane wave, characterized by a wavenumber vector $k_x = -0.25$ rad/m and $k_y = -0.4$ rad/m and temporal frequency = 10 Hz, propagating past a circular array of 16 sensors. Figure 4.15 shows the array geometry, and Figure 4.16 shows the corresponding coarray. The ASF is shown in Figure 4.17, and a slice along the k_x axis is shown in Figure 4.18. Notice a large sidelobe occurs at an approximate wavenumber $k_x = 1.95$ rad/m.

The resulting power output of the FDBF is shown in Figure 4.19, and the actual signal location is shown with an asterisk. The FDBF estimates the correct wavenumber, exhibits a large radius around the peak power spectrum estimate, and has some sidelobe or background energy in the upper right portion of the spectrum. The MVDL power

spectrum estimate, shown in Figure 4.20, also predicts the correct wavenumber vector, while exhibiting a significant decrease in the radius around the signal peak. Additionally, the MVDL method has reduced spectrum energy estimated at areas remote from the actual signal energy. The increased resolution of the MVDL method is evident in this synthetic wavefield example.

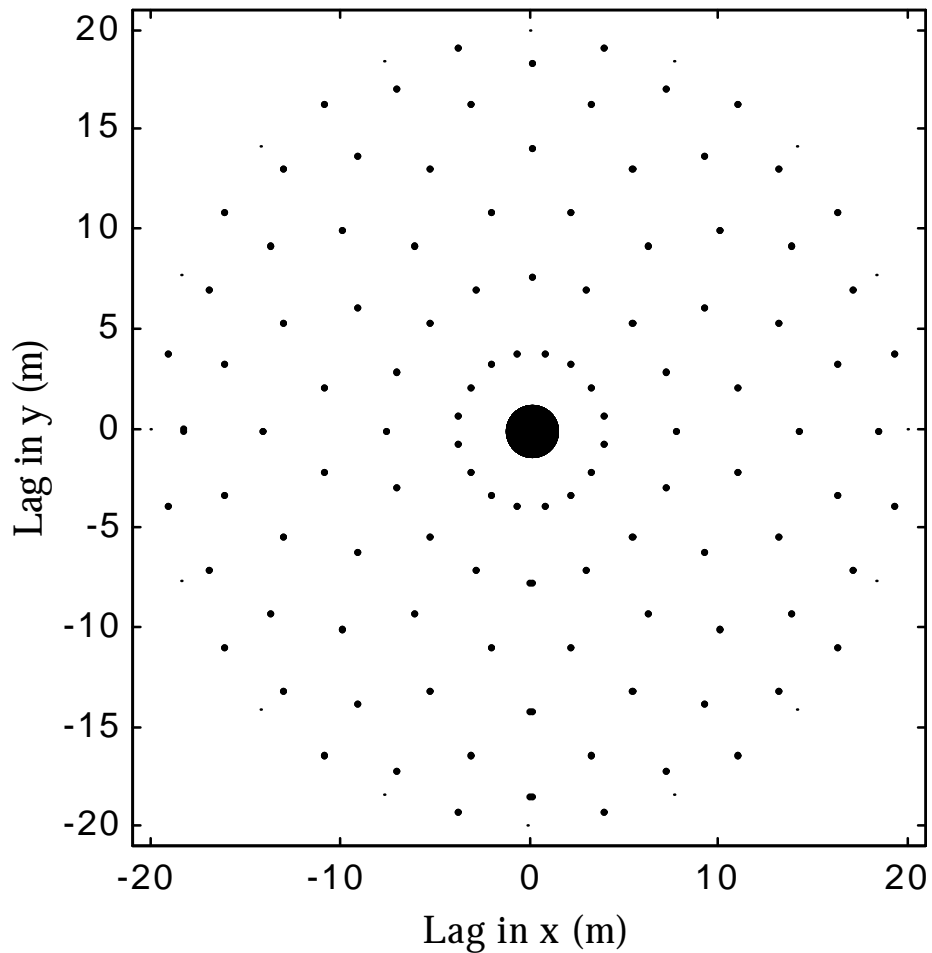


Figure 4.16 Coarray for the 16 Sensor Circular Array Shown in Figure 4.15

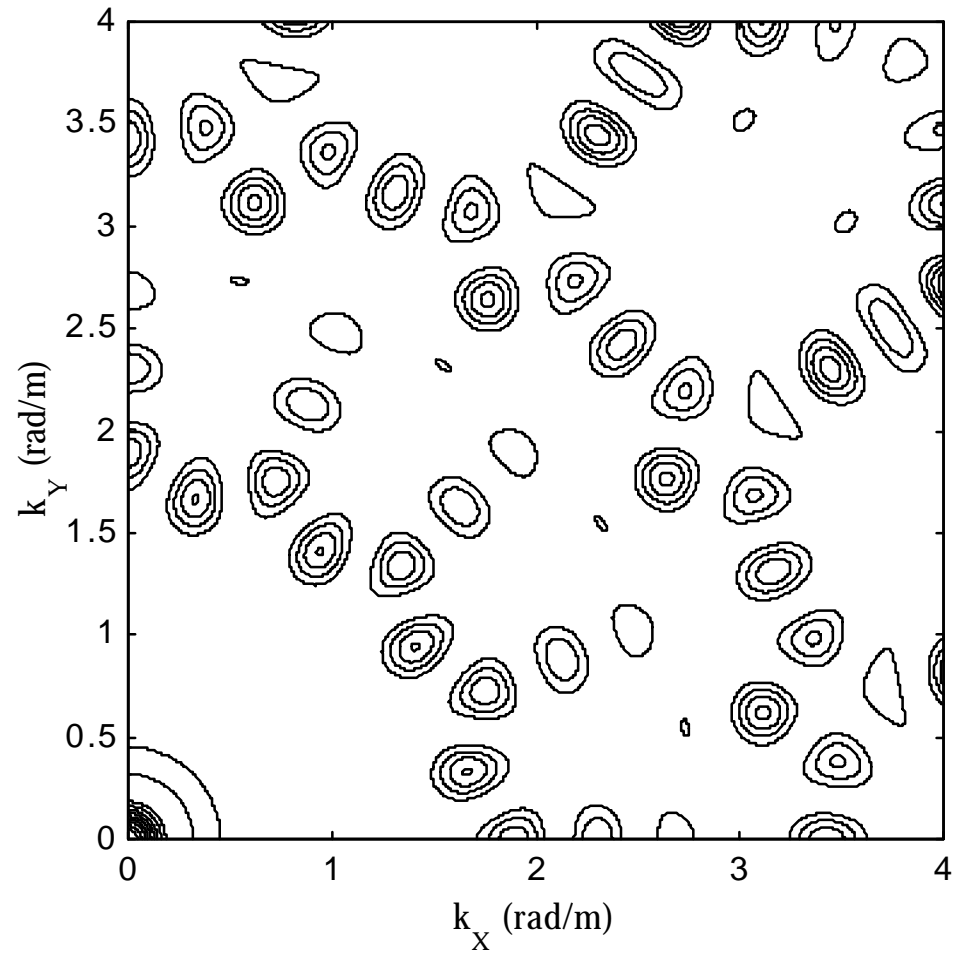


Figure 4.17 Array Smoothing Function for the 16 Sensor Circular Array

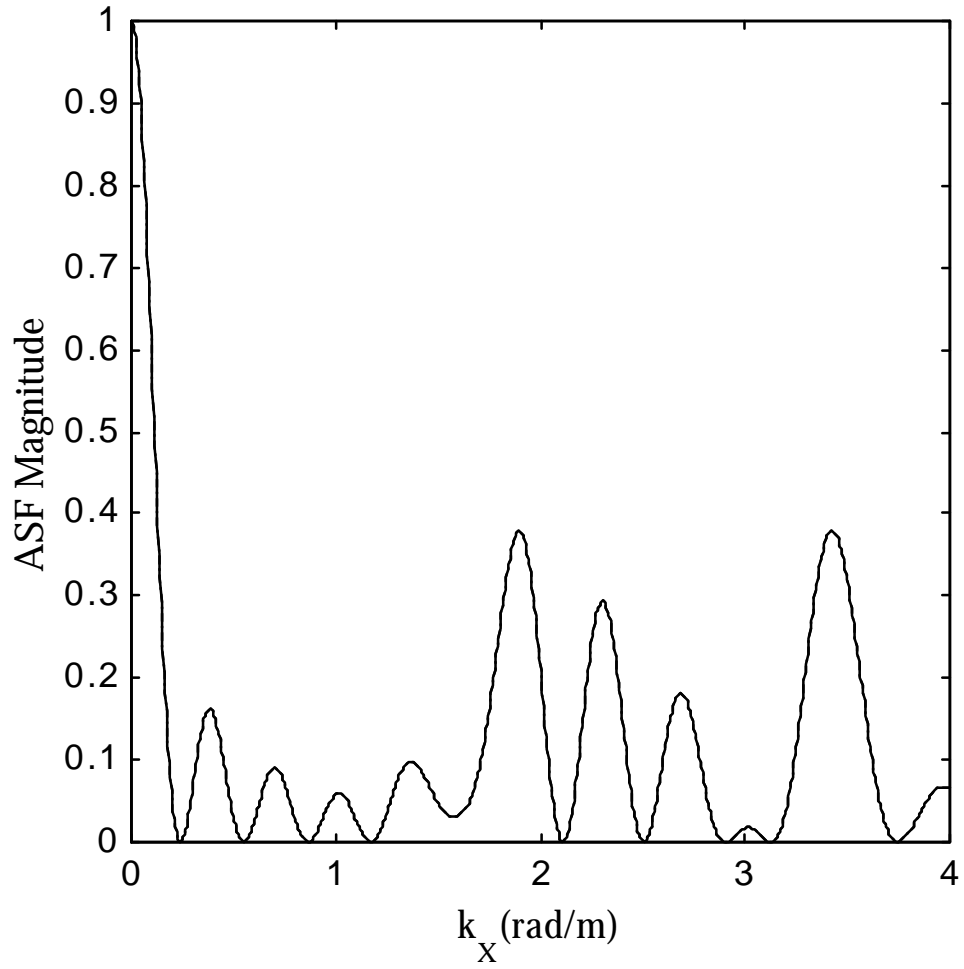


Figure 4.18 Slice of the Array Smoothing Function Shown in Figure 4.17 Along the k_x Axis. Due to symmetry and the orientation of the array, the orthogonal slice along the k_y axis is identical to the slice shown.

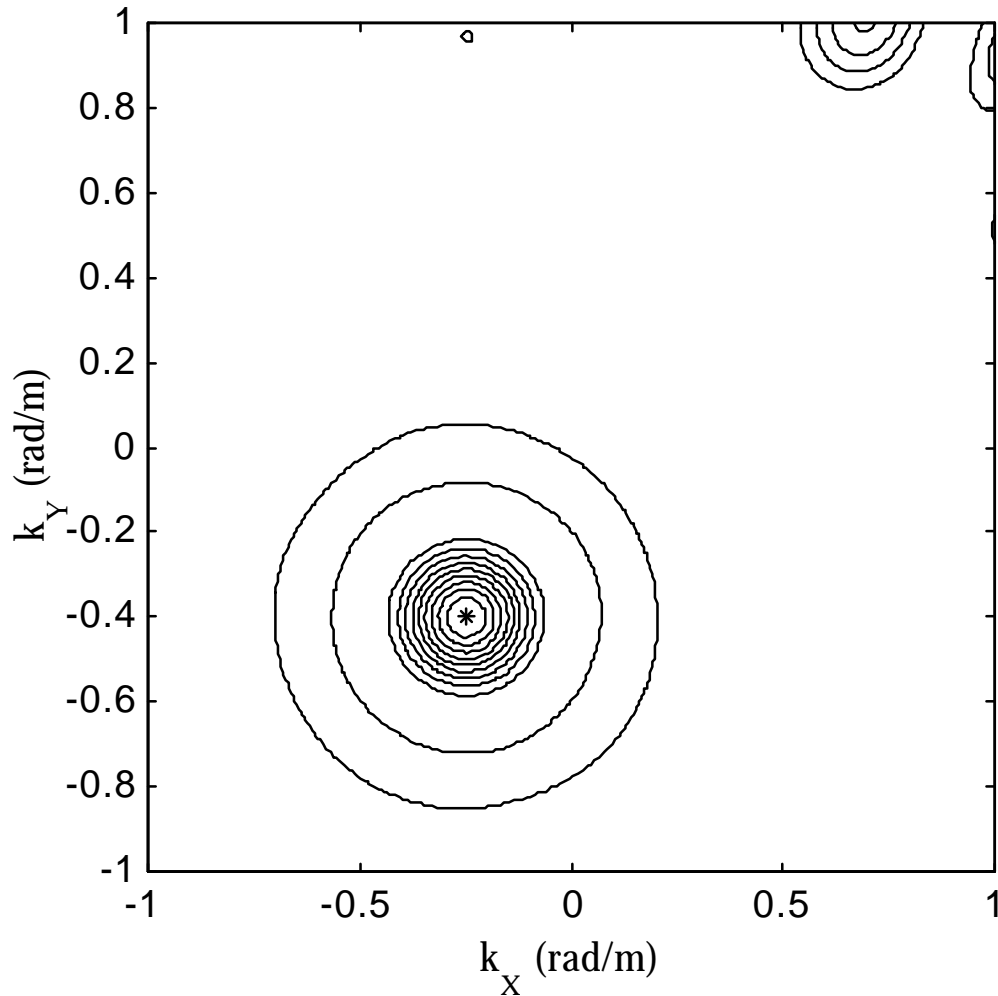


Figure 4.19 Frequency-Wavenumber Spectrum Estimate from the FDBF for a Single Wave Propagating with a Wavenumber $k_x = -0.25$ and $k_y = -0.4$ rad/m and Frequency = 10 Hz. The asterisk indicates the true propagation wavenumber.

4.7 Spatial and Temporal Domain Parallels

Many parallels between the one-dimensional and multidimensional problems exist. The parallels not only help extend the signal processing algorithms and theory to problems with larger dimensions, but also emphasize the primary functions and parameters of interest. Table 4.2 shows the functions and parameters outlined in Chapters 3 and 4 for the one-dimensional and multidimensional cases.

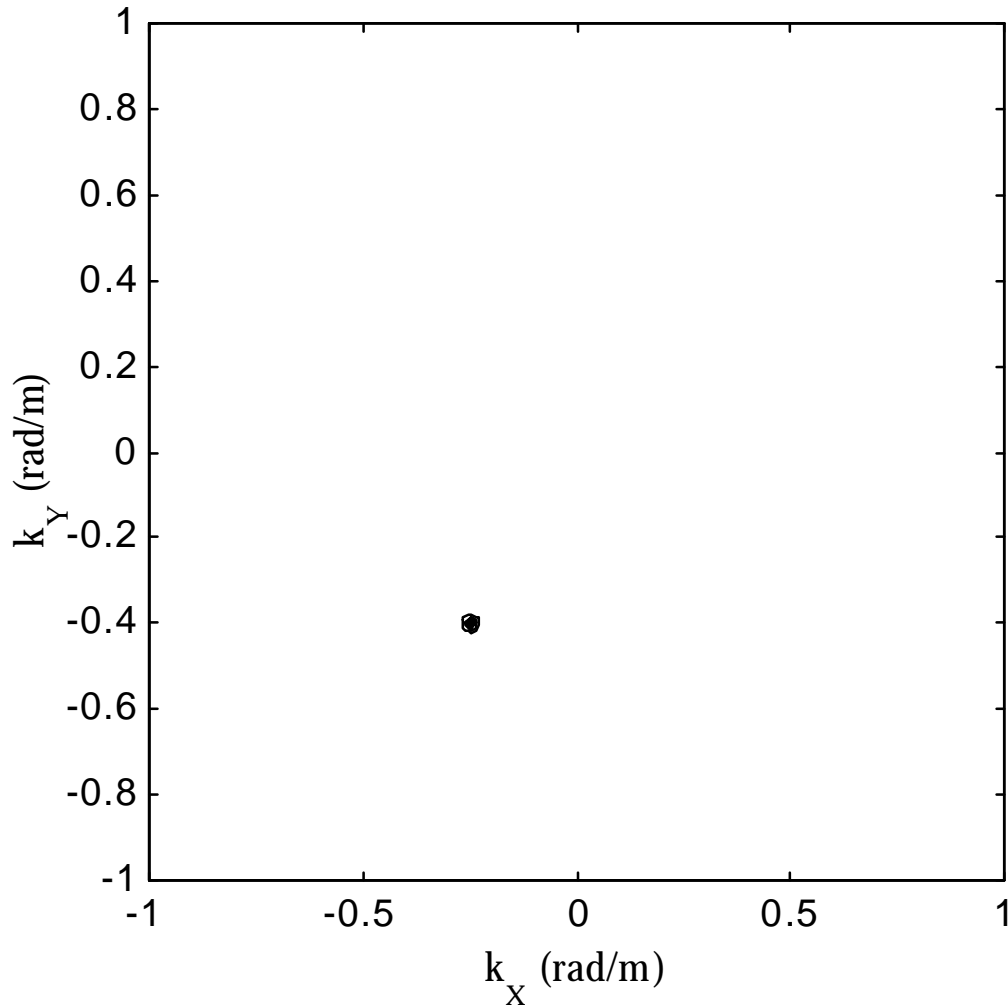


Figure 4.20 Frequency-Wavenumber Spectrum Estimate from the MVDL Method for a Single Wave Propagating with a Wavenumber $k_x = -0.25$ and $k_y = -0.4$ rad/m and Frequency = 10 Hz

4.8 Summary

Spatiotemporal signal processing allows a great deal of information to be extracted from spatial wavefields. The primary problem in multidimensional signal processing remains the same as in the one-dimensional case -- design an optimum filter to sift out desired information from experimental measurements. Several power spectrum estimators were discussed. The frequency domain beamformer (FDBF) offers the easiest method of implementation, but in many cases, more advanced methods, such as MVDL, linear prediction, and MUSIC, offer the optimum solution.

Table 4.2 Temporal and Spatiotemporal Signal Processing Parallels

	Temporal	Spatiotemporal
Lag Domain	t_s and N	Coarray
Weight Vector, $w[n]$	Sample weight	Sensor weight
Function of Interest	Correlation r	$R(\omega)$
Simple Power Spectrum Estimate	Periodogram	FDBF
Approximate Resolution	$\Delta\omega = \frac{2\pi}{\text{Window Length}}$	$\Delta\mathbf{k} = \frac{2\pi}{\text{Array Length}}$
Aliasing	$\omega_{\max} = \frac{\pi}{t_s}$	$\mathbf{k}(\vec{\zeta})_{\max} = \frac{\pi}{d_{\min}(\vec{\zeta})}$

Simple wavefield examples, containing only a single signal, showed the applicability of the algorithms, and displayed the superior power of the advanced spectrum estimation methods. In practical applications, the wavefield may contain non-ideal components that deteriorate the performance of any or all of the spectrum estimators. The noise field characteristics may be white or colored, i.e. correlated between sensors, and noise characteristics may differ for various spatial and temporal scales. Multipath propagation adds an additional concern, since the same signal may produce two closely spaced and correlated signals, which will deteriorate the performance of the spectrum estimators, especially adaptive methods that seek to null out competing signals.

The array smoothing function, analogous to the one-dimensional smoothing kernel, controls the spectral properties of the array. The spatiotemporal resolution and aliasing criteria are very similar to the one-dimensional temporal criteria, relying on the maximum and minimum spatial sampling lag. If the array smoothing function has poor sidelobe control, then sidelobe interference becomes a great concern in wavefields containing multiple signals. In previous geotechnical spatial array processing applications, the array smoothing function has received little attention and analysis. To adequately analyze the power spectrum of a spatiotemporal wavefield, especially when sampling with a limited number of sensors, the array smoothing function must be analyzed to determine where large sidelobes and grating lobes occur.